

## The Use of Multispectral Infrared Thermography in Re-entry Vehicles

by C. Pereira\*, T. Roesgen\*\*, S. Walz\*, S. Airaghi\*\*

\*RUAG Space, Schaffhauserstr. 580, 8052 Zurich, Switzerland , [carlos.pereira@ruag.com](mailto:carlos.pereira@ruag.com)

\*\* Institute of Fluid Dynamics, Sonneggstr. 3, 8092 Zurich. Switzerland, [roesgen@ifd.mavt.ethz.ch](mailto:roesgen@ifd.mavt.ethz.ch)

### Abstract

This paper describes the design of a second generation infrared thermography system for use in a re-entry vehicle. Due to the large number of contaminants such as hydrazine and partial oxidation of the surfaces the simultaneous observation of temperature and emissivity must be performed. To this end a multispectral concept was validated in laboratory tests and implemented in the design.

### 1. Introduction

Control surfaces of re-entry vehicles are subject to thermal loads caused by high enthalpy flows (figure 1). The measurement of these flows traditionally relies on thermocouple grids. The poor spatial and temporal resolution of these grids does not allow an accurate thermal mapping of the surface or a reconstruction of front face temperatures [1]. The chosen measurement method in the Intermediate eXperimental Vehicle (IXV) of the European Space Agency (ESA) is near infrared thermography [2].

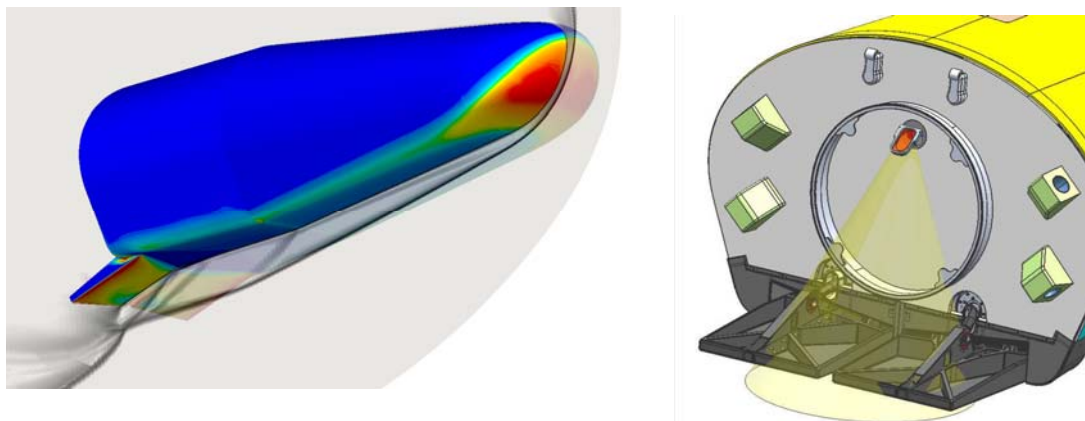


**Fig. 1.** Heating of IXV during Re-entry. (Courtesy: CFS Engineering) and Periscope Optics for Flap Observation

In re-entry vehicles the emissivity will vary due to presence of contamination, oxidation and angular position of control surfaces so a simultaneous measurement of the emissivity and temperature is required. Thermocouples placed on the surface can be used to fit the data, as shown in [3] but complicated flap design limits their usefulness for this correction. Furthermore control surfaces such as ailerons or rudders cannot incorporate a large number of thermocouples without increasing the torque necessary to move them. In this case a multispectral measurement will deliver simultaneous measurement of temperature and emissivity without the need of reference thermocouples.

## 2. Background

Starting with the Planck distribution in the “short wavelength” limit, one may write an equation (Eq. 1) containing the logarithmic emissivity and the *inverse temperature*,

$$\log[G\varepsilon_0] - \frac{C_2}{\lambda_i T} = \log\left[\frac{I_{\lambda_i} \lambda_i^5}{\Phi(\lambda_i) C_1}\right] \quad (1)$$

Where,  $G$  is the pixel conversion gain,  $\Phi$  the filter specific transmission and  $\varepsilon$  is the target emissivity. The term on the right hand side contains the measurement values and otherwise known constants. With measurements at two different wavelengths one obtains a system of two linear equations which can be solved if  $\lambda_1 \neq \lambda_2$ .

$$\log\left[\frac{I_{\lambda_i} \lambda_i^5}{\Phi(\lambda_i) C_1}\right] = \log[G\varepsilon_0] - \frac{C_2}{\lambda_i T}$$

$$\begin{bmatrix} 1 & -\frac{C_2}{\lambda_1} \\ 1 & -\frac{C_2}{\lambda_2} \end{bmatrix} \begin{bmatrix} \log(G\varepsilon_0) \\ \frac{1}{T} \end{bmatrix} = \begin{bmatrix} \log\left(\frac{I_{\lambda_1} \lambda_1^5}{\Phi(\lambda_1) C_1}\right) \\ \log\left(\frac{I_{\lambda_2} \lambda_2^5}{\Phi(\lambda_2) C_1}\right) \end{bmatrix} \quad (2)$$

From an implementation point of view two measurement systems can be used: a mosaic pixel referenced filter placed in the image plane or a filter wheel.

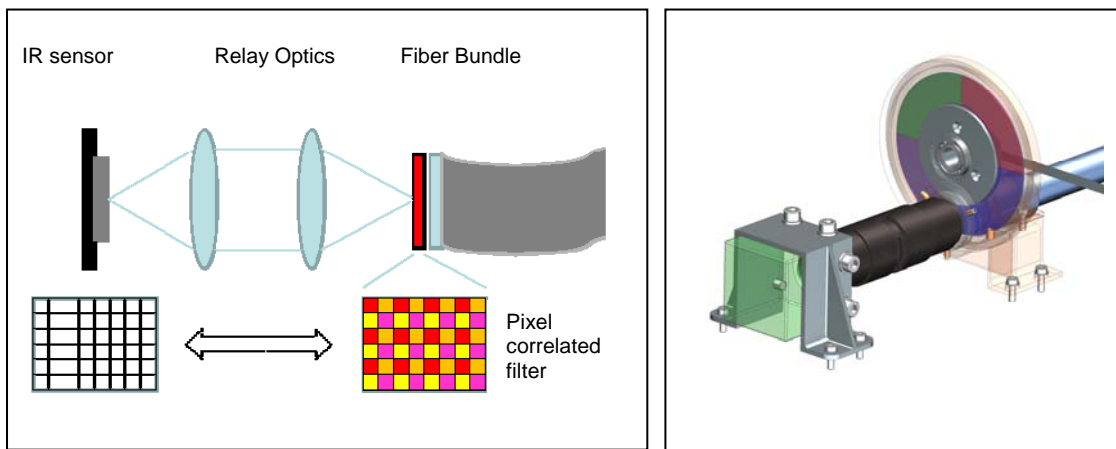


**Fig. 2. Alternative Multispectral Concepts**

## 3. Concept Demonstration

The multispectral filter is ideally a mosaic pattern with a repeating pattern of pixel-sized optical band pass filters. While this is technically feasible, it was decided to use a simplified configuration with three band pass filters arranged in parallel stripes. This will not allow for a full resolution recording of images but should be sufficient for the analysis of surface segments with uniform but still unknown temperatures and emissivities.

Figure 3 shows the arrangement of the filter stripes and the spectral characteristics of the band pass filters.

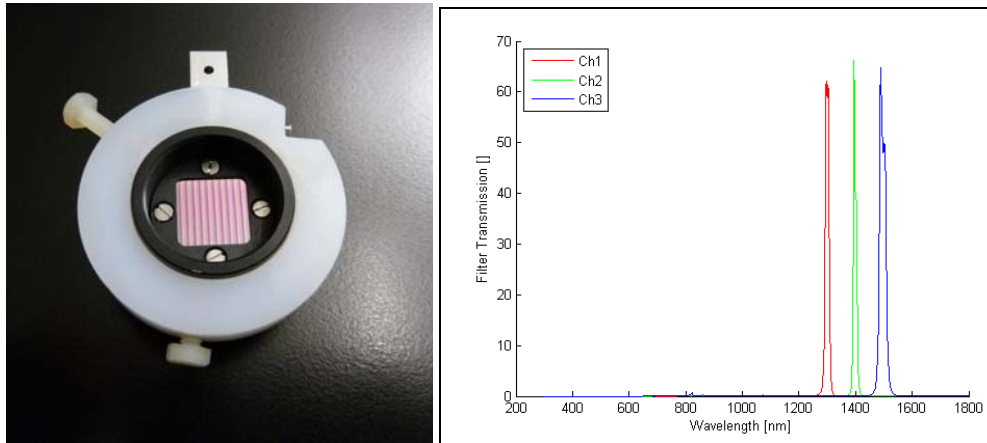


Fig. 3. Layout of the optical stripe filter

The test target consisted of two sample plates, each with a size of 95 mm x 95 mm. One plate was made of C/SiC, the other of Inconel<sup>®</sup>, thus presenting two targets with different emissivity. The samples were inserted into the insulated aperture of a high temperature oven (see Figure 4). Significant for the results is the fact that the samples were supported by a rear carrier plate with a round aperture. This leads to a non-uniform heating and emission of the sample surfaces and has to be taken into account during the analysis. Figure 4 presents a schematic of the sample installation with the ceramic holder.

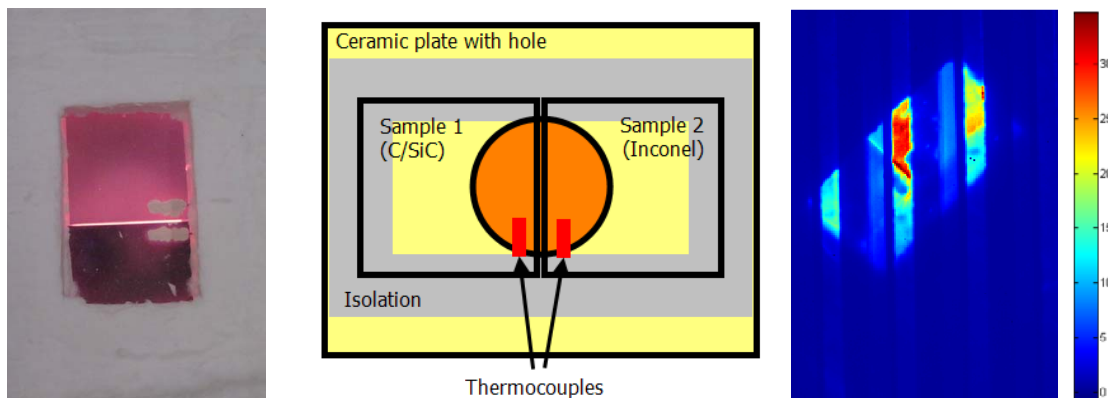


Fig. 4. Multispectral Infrared Testing

A typical experiment run consisted in heating the oven to a set temperature with the sample aperture covered. Following removal of the aperture cover, the sample would cool down due to the increased radiation heat loss to the environment. This decay in sample temperature was monitored with the thermocouples, and the IR camera recorded the image scene simultaneously through the multi-wavelength stripe filter.

Before any quantitative processing of the image data can be performed, a number of calibration steps have to be applied. First, a standard background and flat field correction are performed, using the formula

$$I(x, y, T_{obj}) = \frac{S(x, y, T_{obj}, T_{cam}) - B(x, y, T_{cam})}{G(x, y, T_{cam})} \quad (3)$$

where,  $I(x, y, T_{obj})$  denotes the corrected image intensity,  $S(x, y, T_{obj}, T_{cam})$  is the raw signal,  $B(x, y, T_{cam})$  the background signal and  $G(x, y, T_{cam})$  the (relative) pixel gain. Note that the offset and gain functions depend on the camera temperature. Both functions are obtained during a separate calibration procedure using the camera's dark noise pictures at different temperatures and exposure times.

One important detail to notice is that the target surfaces are not the only hot surfaces radiating in the image. Rather, the sidewalls of the oven insulation in the aperture cutout act as reflectors and produce also a significant infrared radiation signal. Thus the bottom third of the visible hot regions (towards the lower right of the image) has to be discarded in the target surface image analysis. Also visible are “dead” and “hot” pixels, two typical blemishes specific to individual IR sensors.

The final image calibration step is the division by a pixel-dependent gain function, designed to remove any remaining non-uniformities in the pixel gain. Figure 5 shows the output image, which is used in the scene dependent geometric and spectral analysis. The large stripe pattern remaining visible in the image is now solely due to the varying transmission characteristics of the three color stripe filters.

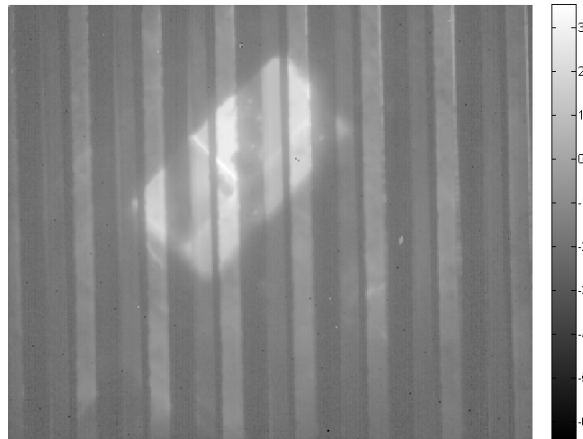


Fig. 5. Intensity Corrected Image

In order to derive temperatures from relative pixel intensities, two external factors have to be removed which affect the spectral response of the camera. The three optical band pass filters realized in the stripe patterns affect the recorded intensities in two ways. First, the *peak transmission* may vary between the filters and has to be corrected for. The same holds also for the filters' *bandwidth*. An easy way to compute the relevant correction factors is to look at the integral transmission curves, defined here as

$$\Phi(\lambda) = \int_0^\lambda \tau(\xi) d\xi \tag{4}$$

where  $\tau(\lambda)$  is the spectral transmission curve. The integral value  $\Phi$  captures both the peak height of the transmission curve as well as its width. This result is shown in Figure 6. One recognizes that the response is not monotonic. Filter 2 has the lowest integral transmission because of its comparatively small bandwidth. The relative weight of the three filters is simply the asymptotic value of  $\Phi(\lambda \rightarrow \infty)$ .

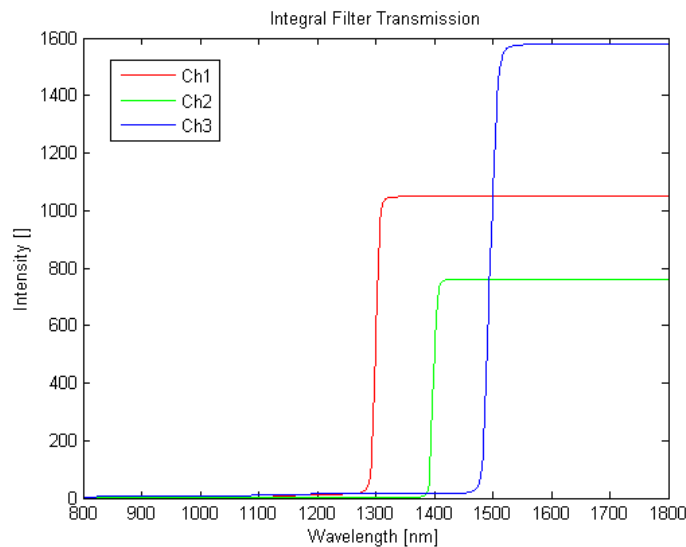
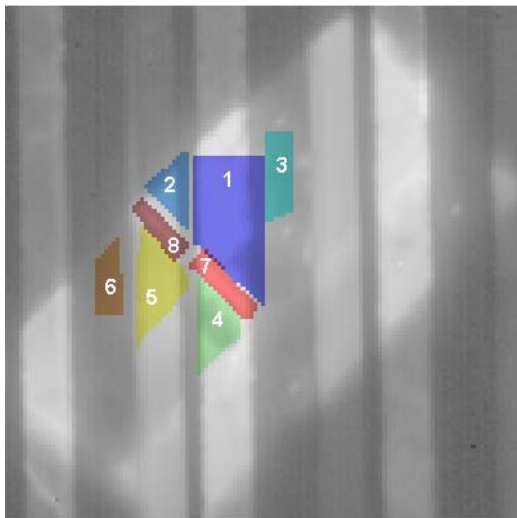


Fig. 6. Integral Filter Transmission Curves

The main assumption underlying the spectral processing of the image data is that the target scene's emission does not change significantly across the different filters. While a full mosaic filter would produce different wavelength readings effectively at the pixel level, the stripe filter used in the present verification test has a finite filter strip width which extends across several pixel columns. Given the comparatively large size of the stripe pattern this implies that the scene viewed by the IR camera should have an approximately uniform intensity across the two targets. This is unfortunately not fulfilled because of the ceramic support aperture. The aperture effect can be seen for example in Figure 4, where the apparent brightness of the image changes significantly across the two tile segments.

Thus, any form of spatial averaging of image segments under the assumption of equal temperatures is dangerous. On the other hand, relying on individual pixel values is equally problematic because of noise, optical contamination of the filters and other spatially varying error sources. As a compromise, the processing will be based on the *maximum normalized intensity values found in polygonal regions of interest*. Picking the maximum value is reasonable because most error sources will normally lead to a reduction in intensity. Given the geometric constraints of the filter stripes, the maximum is thus a good estimate of the least disturbed measurement value in the respective regions of interest. Figure 7 shows the regions of interest for the two tiles and the gap region in between. In the gap (patches #7 and #8) the radiation of the oven cavity is directly visible, providing a convenient temperature reference with nearly black body characteristics. The sampling patches in the image are associated with the three different filters. The correspondences are listed in the table.



Patch	Sample	Filter	Wavelength [μm]
1	1	3	1.5
2	1	1	1.3
3	1	2	1.4
4	2	3	1.5
5	2	1	1.3
6	2	2	1.4
7	Oven	3	1.5
8	Oven	1	1.3

Fig. 7. Sampling patches in the target scene and filter correspondence

Solving equation 2 for the different filters results in the two graphs for heating and cool-down of figure 8.

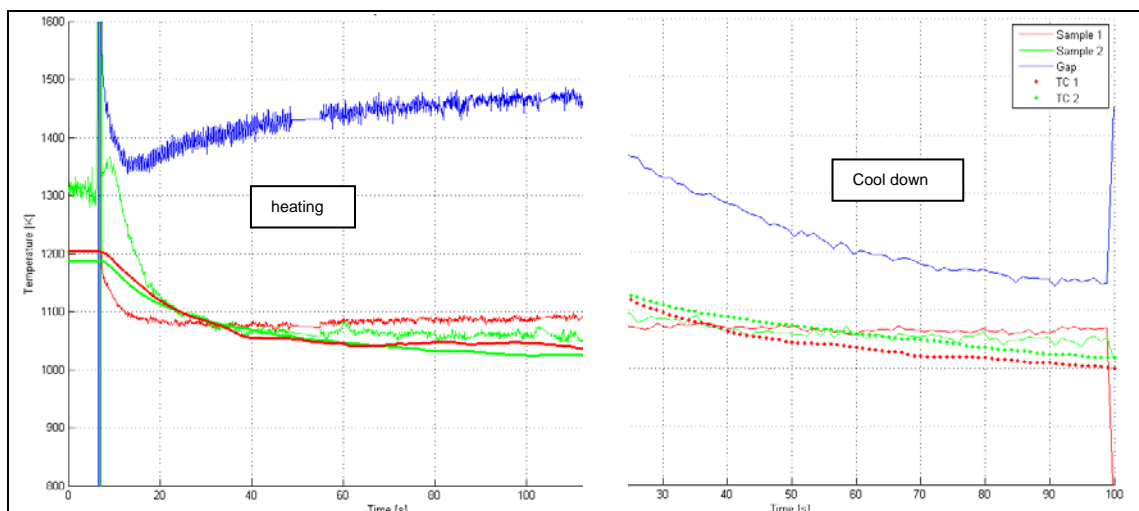


Fig. 8. Measured Temperatures (Multispectral IR and Thermocouple Data)

The correlation of the measurement with the thermocouple data is good. An interesting observation is that the IR measurements show different time constants for the temperature adjustment of the two samples, whereas the thermocouples register almost identical decays. It appears that Sample 1 (Inconel®) is cooling down faster than the C/SiC Sample 2.

#### 4. Filter Design

The most severe drawback in the present demonstration proves to be the comparatively low spatial resolution of the stripe filter pattern in combination with significant temperature variations on the target surfaces. This limits the accuracy to which the temperatures could be reconstructed. As a recommendation, one should design the final filter mosaic with a pitch of a single camera pixel, thus maximizing the achievable spatial resolution and registration capability. The main problem of the pixel correlated filter is maintaining the initial alignment between the filter position and the detector, a non trivial problem given the high mechanical and thermal loads on the system.

As an alternative, one may consider the rotating filter wheel. Here, the spatial registration of the filter channels will be perfect, at the cost of a slightly reduced temporal resolution. As the IR camera proposed for IXV can be operated at frequencies beyond 25 Hz, this should not represent a significant constraint, though. The feasibility has been shown in the low temperature region in [4] however a rotating system poses problems of its own, namely the ability to sustain mechanical loads and the synchronisation of the camera with the rotating filter.

While filter wheels are common in digital light processing they are less so in the infrared. However the alignment problems of the pixel correlated grid were so large that it was decided to switch to a filter wheel system. The main considerations that apply are: the performance of the filter wheel in the near infrared, the synchronization of the wheel to the detector and the ability to withstand environmental loads.

The previous work documented above as well as in [4] indicates that a two wavelength filter suffices to establish a thermal map of the flap surface which is expected to be partially oxidized and coated with ablative char. For the IXV experiment it was decided to use three wavelength (or "color") filter. If the filters are sufficiently narrow band, the wavelength integrated response becomes

$$I(\lambda, \Delta\lambda, T) \approx \frac{2hc^2}{\lambda^5} \exp\left(\frac{-hc}{\lambda k_B T}\right) \Delta\lambda \quad (5)$$

One may evaluate the *relative* response of the sensor for a pair of wavelengths and bandwidths,

$$r = \frac{I(\lambda_1, \Delta\lambda_1, T)}{I(\lambda_2, \Delta\lambda_2, T)} \approx \frac{\lambda_2^5}{\lambda_1^5} \exp\left(\frac{-hc}{k_B T} \left[ \frac{1}{\lambda_1} - \frac{1}{\lambda_2} \right]\right) \frac{\Delta\lambda_1 s_1}{\Delta\lambda_2 s_2} \quad (6)$$

with the response values "s" for the candidate wavelengths are listed in the table below.

**Table 1.** Camera response for narrow filter set

Center Wavelength [nm]	Photoresponse [A/W]
1490	1.03
1550	1.04
1610	1.02
1670	0.86

In order to visualize the effect of wavelength and temperature on the relative sensor response, the bandwidth ratio  $\Delta\lambda_1/\Delta\lambda_2$  can be formally set to unity, and the rest of the relation is evaluated. The result is shown in figure 9.

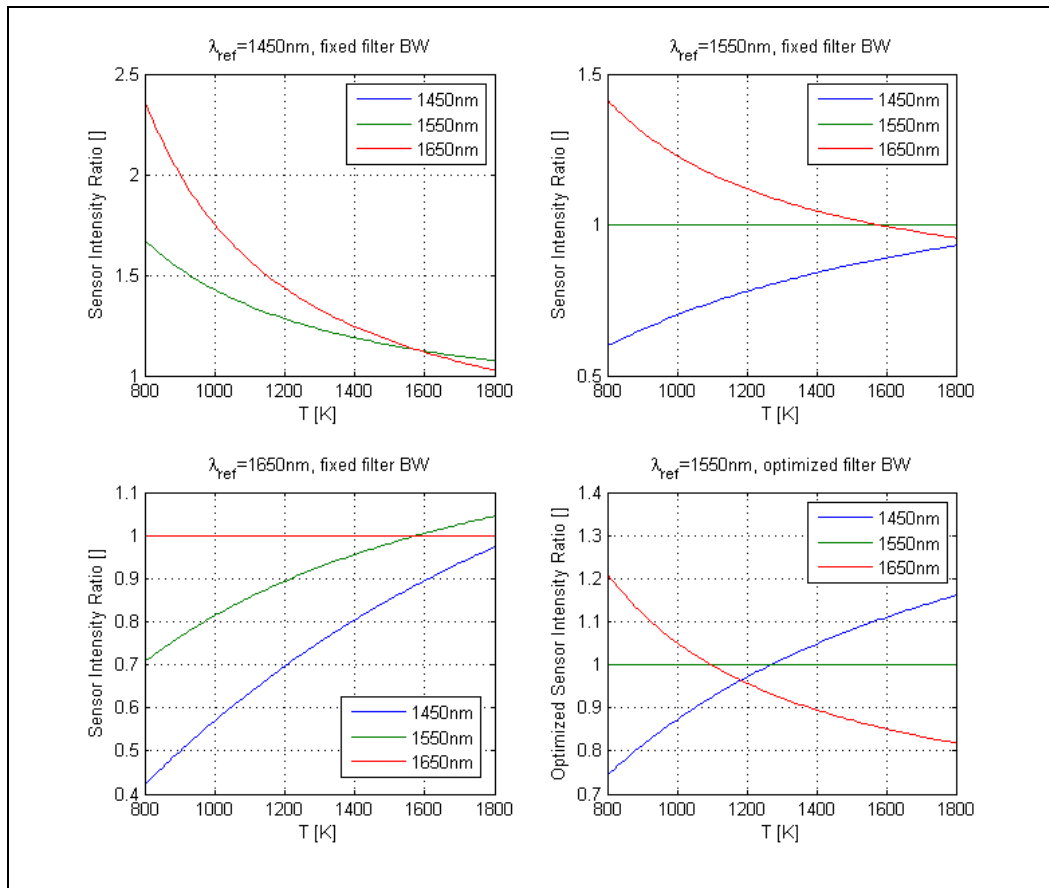


Fig. 9 Sensor response for different filters

One recognizes that the relative responses vary in the range 0.4 - 2.5 dependent on the choice of the reference wavelength. This represents an important number because it defines the minimum required dynamic range of the sensor so that it can record signals from two filter wavelengths with a single exposure time in the complete temperature range (800 K – 1800 K).

Table 2. Maximum intensity ratios for different filter combinations.

CWL [nm]	1450	1550	1650
1450	1.0000	1.5598	2.3054
1550	1.5598	1.0000	1.4780
1650	2.3054	1.4780	1.0000

The numbers appear reasonable for all filter combinations.

The filter set performance might still be improved slightly by adjusting the filter bandwidths. Performing an optimization of the relative filter bandwidths by minimizing the overall squared difference in the relative intensity ratios gives the values listed in Table 3. The absolute bandwidths are computed by using the value of 10 nm for the longest wavelength, a value close to the one used in the filter design of the EXPERT re-entry experiment.

Table 3. Optimized Filter Bandwidths

CWL [nm]	1450	1550	1650
Rel. bandwidth	1.246	1.00	0.855
Abs. bandwidth [nm]	14.6	11.7	10.0

For the realization of the filter wheel solution the synchronisation between the filter wheel and the camera image acquisition is of main importance. In order to minimize possible errors and delays a direct synchronisation is preferred.

For the camera a version with external trigger exists which allows direct control of the image acquisition with a maximum of 100 Hz. The external trigger signal to apply is a TTL +5.0 V input, low level is 0 V.

The trigger signal will be generated by Hall sensors integrated on the filter wheel. Three sensors are foreseen, one for each filter segment. On the rotor one magnet and one non-magnetic counter balance will be integrated. While the sensor signals will be transferred to the Data Handling Unit (DHU) for orientation determination a superposed sensor signal will be used for the camera triggering. With this concept the absolute position of the filter wheel can be determined by the DHU while the camera in parallel receives a direct triggering signal from the filter wheel. The DHU will be able to tag each image with filter position. The schematic of the sensors and the triggering signal is shown in figure 10.

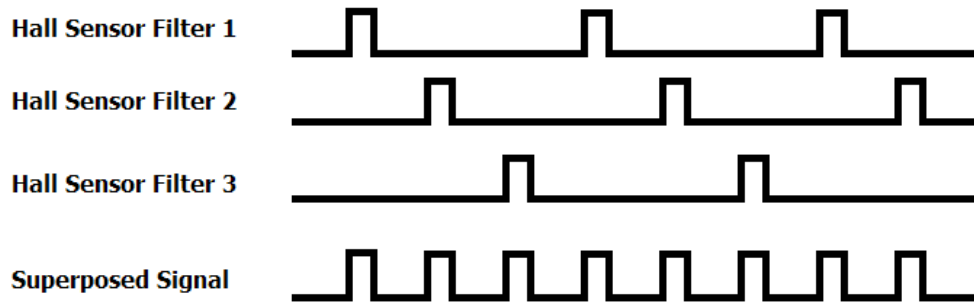


Fig. 10 Hall sensor synchronization signal concept.

Figure 11 shows the connection diagram for the whole IR camera experiment with the filter wheel.

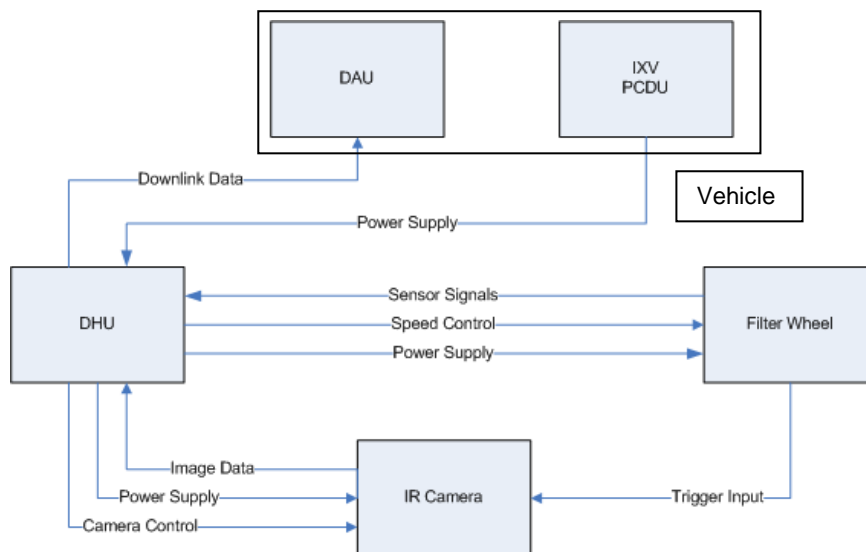


Fig. 11 System Design

In this design the filter wheel triggers the camera and sends position information to its data handling unit (DHU). This unit compresses the images and sends them to the vehicle data acquisition unit (DAU) while storing raw data images in its redundant solid state memories. It also conditions the power from the vehicle power distribution unit (PCDU) for both the filter wheel and camera. Speed control and recovery modes (back-up triggering mode) are also managed by the DHU.

Thus the synchronization issue is reduced to an alignment issue of the filter wheel disc to the installed hall sensors. This alignment can be handled on ground during integration and allows optimum functional testing capabilities.

## 5. Conclusions

A multispectral thermography system was developed for use in the IXV vehicle in order to measure emissivity and temperature simultaneously. The concept was validated using line filters and further expanded to the use of a filter wheel due to its higher reliability and spatial resolution. The filter wheel design has successfully passed environmental testing and it is undergoing qualification testing within the IXV programme.

## Acknowledgements

The authors wish to thank the Swiss Space Office and the European Space Agency for their support as well as Thales Alenia Spazio in Torino for the collaborative effort.

## REFERENCES

- [1] Rouzaud, O. et. al. (2005). "Assessment of the Thermal Inverse Method Applied to EXPERT Closed Flap", ONERA RT 2/09428 DMPH/DMAE
- [2] S. Walz, T. Roesgen, C. Pereira, K. Handrick, A. Steinacher;"Design and Validation of a Temperature Measurement System for the Movable Flaps on the IXV", Proceedings of the 7th European Symposium on Aero-Thermodynamics for Space Vehicles, Brugge (2011).
- [3] T. Roesgen, C. Pereira, S. Airaghi, A. Vuilleumier, "Temperature Mapping of a Re-entry Vehicle Flap in High Enthalpy Flow Test", Proceedings of 11th Quantitative InfraRed Thermography conference, paper QIRT2010-234 Naples (Italy), 2012
- [4] T. Gruenberg, "Laser Assisted Multispectral Imaging Pyrometry for Thermometry on Surfaces with Variable Emissivity", Diplomarbeit ILR-RSN DA 10-03, ETH Zurich (2010).